

## A Small-Angle X-ray Scattering Apparatus for Studying Biological Macromolecules in Solution

ZIMEI BU, ARTHUR PERLO, GERALD E. JOHNSON, GERALD OLACK, DONALD M. ENGELMAN\* AND HAROLD W. WYCKOFF  
*Department of Molecular Biophysics and Biochemistry, Yale University, 260 Whitney Avenue, PO Box 208114, New Haven, CT 06520-8114, USA. E-mail: don@paradigm.csb.yale.edu*

(Received 30 May 1997; accepted 3 November 1997)

### Abstract

This paper describes the development of a simple laboratory-based small-angle X-ray scattering apparatus for the study of biological macromolecules in solution. The instrument is based on a two-circular-aperture collimation design combined with a conventional rotating-anode Cu  $K\alpha$  X-ray source, a graphite monochromator and a multiwire area detector. The geometry of the collimator, the beam-stop-to-detector distance and the thickness of the platinum foil of the defining aperture have been optimized to reduce background scattering. The effective  $Q$  range is from 0.01 to  $0.33 \text{ \AA}^{-1}$ , where  $Q = (4\pi \sin\theta)/\lambda$  is the magnitude of the scattering vector,  $2\theta$  is the scattering angle and  $\lambda$  is the wavelength of the X-rays. The length of the collimator, the pinhole sizes and the helium-flushed sample-to-detector path can be easily changed depending on the resolution and intensity requirements of an experiment. The diffraction pattern of a polycrystalline pellet of ammonium sulfate mounted about 2.5 cm in front of the beam stop and 40 cm in front of the detector is used to monitor changes in the incident-beam intensity as well as the differences in absorption of X-rays by the sample solutions and the solvents, to ensure correct background subtractions. Data collection is controlled by a computer through a parallel DMA (direct memory access) I/O module. Data collection and reduction software has been developed. The typical data collection time is about 2 h for a  $5 \text{ mg ml}^{-1}$  10 kDa protein dissolved in an aqueous solution. Examples of applications of this small-angle X-ray scattering instrument to studying protein size and conformation changes are presented.

### 1. Introduction

Small-angle X-ray scattering (SAXS) is a useful technique for obtaining structural information from macromolecules. The length-scale range readily probed by SAXS makes it especially suitable for measuring the size, shape and molecular weight of proteins and nucleic acids with radii of gyration ( $R_g$ ) of 10–50 Å and maximum dimensions ( $D_{\text{max}}$ ) of 20–300 Å. Examples of applications include studying conformational changes,

protein folding/unfolding, ligand-induced oligomerization and enzyme–substrate interactions (Guinier & Fournet, 1955; Pessen *et al.*, 1973; Glatter & Kratky, 1982; Moore, 1982; Flanagan *et al.*, 1993; Kataoka *et al.*, 1993; Lattman, 1994; Tuzikov *et al.*, 1996; Lemmon *et al.*, 1997). SAXS can also be used for diffraction studies of the dimensions and phase transitions of biological membranes and lipid bilayers (Lewis & Engelman, 1983; Tournois *et al.*, 1987; Batenburg *et al.*, 1988; Hare *et al.*, 1995).

The scattered intensity from a solution of biological macromolecules is usually weak because the electron-density contrast between a macromolecule, *e.g.* a protein, and its aqueous buffer is low. Further, the experiment is conducted in a dilute solution to reduce the effect of intermolecular interactions. The weak scattering requires that the X-ray flux of an SAXS apparatus be maximized and the background scattering be minimized. The minimum accessible angle must be small enough to permit measurement of macromolecules with  $D_{\text{max}}$  of 10–300 Å. Maximizing flux consistent with a resolution requirement is especially important when a conventional rotating-anode X-ray source is employed, or measurement times will be unacceptably long. At the same time, the apparatus should be flexible enough to allow easy optical geometry changes to adjust to different resolution requirements.

A beam monitor is required to monitor beam-intensity changes and the differences in absorption/transmission of X-rays by the sample to ensure correct background subtractions. When measuring the molecular-weight changes of biological molecules, such as the oligomerization of proteins to form a complex, a beam monitor is usually necessary to normalize the scattering data collected from a series of samples for precise molecular-weight determinations. A well collimated circular beam is also desirable for eliminating the need for desmearing procedures when reducing the SAXS data.

Although data acquisition rates are much slower than at a synchrotron source, a laboratory-based SAXS apparatus employing a conventional rotating-anode source is suitable for many of the above purposes. It has the advantages of local availability, source stability and low cost. When an area detector is used, a SAXS

experiment with a conventional source can cover a large solid angle at a given  $Q$  to accumulate more X-ray photon counts to increase the signal-to-noise ratio and to reduce data collection time when compared to a linear detector.

In this paper, we describe the development of SAXS apparatus for studying biological macromolecules in solution. This SAXS apparatus uses a rotating-anode X-ray generator and a multiwire area detector. The beam is collimated by two circular apertures to eliminate the need for desmearing of the scattering data during the data reduction process and to exploit the area-detector capabilities. The thickness of the platinum foil of the defining aperture and the diameter of the collimator tube have been designed to reduce parasitic scattering in the small-angle region. The effective  $Q$  range that can be measured is from 0.01 to 0.33  $\text{\AA}^{-1}$  in a single experiment. The data collection time is about 2 h for a 10 kDa protein dissolved in an aqueous buffer solution at 5 mg ml<sup>-1</sup> for a measurement of the radius of gyration and the forward scattering. A polycrystalline ammonium sulfate crystal pellet was placed about 2.5 cm in front of the beam stop and about 40 cm in front of the detector so that powder rings diffracted from the pellet are not blocked by the beam stop and fall at the edges of the area detector to provide an internal monitor of the integral transmitted beam intensity. The geometry prevents scattering by the beam monitor from striking the detector in the small-angle region. The SAXS apparatus has been successfully applied to studying the conformation and oligomeric state changes of several biological systems (Rodgers *et al.*, 1996; Smith *et al.*, 1996; Lemmon *et al.*, 1997). One difficult example, a study of a small protein unfolding in guanidine hydrochloride solution resulting in low contrast, is described here.

More elaborate two-pinhole-collimated vacuum-based SAXS apparatus using conventional X-ray sources have been constructed at Oak Ridge National Laboratory (ORNL) (Hendricks, 1978; Wignall *et al.*, 1990) and several other places (Yoda, 1984; Hayashi *et al.*, 1988). We show that by optimizing the X-ray flux and resolution, reducing the background scattering and installing a beam monitor, a relatively simple laboratory-based SAXS apparatus can be effectively used for studying weakly scattering proteins in solution.

## 2. Apparatus design considerations

### 2.1. Optimizing the X-ray flux consistent with a required resolution

The starting point of the geometric design was to maximize the flux through the collimator for a given desired resolution. Figs. 1(a) and 1(b) are schematic illustrations of the SAXS station as we have built it. For two apertures with diameters of  $d_1$  and  $d_2$  separated by

$L_1$ , at a distance  $L_2 + L_3$  between the defining aperture  $d_2$  and the detector (see §2.2 for explanations on the gap  $L_3$  between the beam stop and the detector), the scattered intensity  $I(Q)$  registered in an annulus of pixels ( $\Delta Q$ ) in the detector plane centered at a certain  $Q$  has three terms,

$$\begin{aligned} I_s(Q) &= B_s [(\pi^2 d_1^2)/16] (d_2^2/L_1^2) \Delta\Omega \exp(-\mu_s t) t \sigma_s(Q) \\ &\quad + B_s \Pi_s(Q) \exp(-\mu_s t) + \text{Dark}_s \\ &= B_s G T_s t \sigma_s(Q) + B_s T_s \Pi_s(Q) + \text{Dark}_s \end{aligned} \quad (1a)$$

$$\begin{aligned} I_b(Q) &= B_b [(\pi^2 d_1^2)/16] (d_2^2/L_1^2) \Delta\Omega \exp(-\mu_b t) t \sigma_b(Q) \\ &\quad + B_b \Pi_b(Q) \exp(-\mu_b t) + \text{Dark}_b \\ &= B_b G T_b t \sigma_b(Q) + B_b T_b \Pi_b(Q) + \text{Dark}_b \end{aligned} \quad (1b)$$

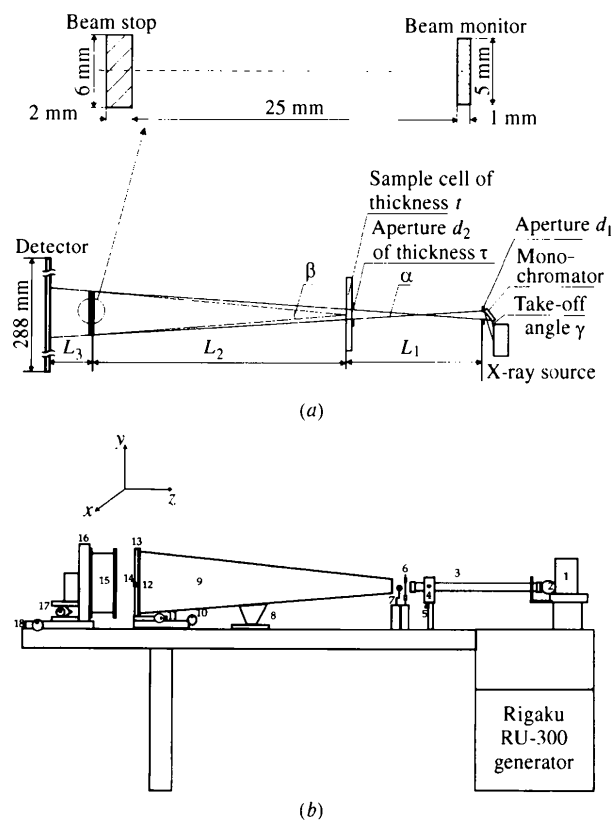


Fig. 1. (a) Diagram of the X-ray optic path. (b) Schematic diagram of the small-angle X-ray scattering apparatus. 1, rotating anode; 2, monochromator (the output port of the monochromator is the input aperture of the collimator); 3, collimator; 4, x translator for the collimator; 5, y translator for the collimator; 6, sample holder; 7, microscope for aligning the samples; 8, support for the helium cone; 9, helium cone; 10, z translator for the helium cone; 11, xy translators for the frame supporting the beam monitor and the beam stop; 12, microscope for aligning the beam monitor and beam stop; 13, frame supporting the beam monitor and the beam stop; 14, beam stop; 15, helium box; 16, SDMS area detector; 17, y translator for the detector; 18, x translator for the detector.

where the subscripts  $s$  and  $b$  stand for the sample solution and the buffer, respectively. The first term in equation (1a) is related to the sample scattering and is a product of the brilliance  $B_s$  of the X-ray source as modified by the monochromator, the geometric factor of the instrument  $G = [(\pi d_1^2)/16](d_2^2/L_1^2)\Delta\Omega$  where  $\Delta\Omega$  is the solid angle of the annulus of width  $\Delta Q$  at a certain  $Q$  in the detector plane, the sample transmission of X-rays  $T_s = \exp(-\mu_s t)$  ( $\mu_s$  is the linear absorption coefficient of the sample), and the scattering cross section of the sample  $\sigma_s(Q)$  per unit volume. The second term,  $B_s \Pi_s(Q) T_s$ , and the third term,  $\text{Dark}_s$ , are the parasitic scattering and the dark count, respectively.

The resolution can be expressed as the largest size of a macromolecule  $R$  that can be measured by SAXS apparatus, which relates to the magnitude of the lowest scattering vector  $Q_{\min}$  by (Glatter & Kratky, 1982; Moore, 1980)

$$R = \pi/Q_{\min} = (\lambda L_2)/2r_{3\min} = [\lambda(L_2 + L_3)]/2r_{4\min} \quad (2)$$

where  $r_{3\min} = r_{3bs} + r_{3bg}$ ,  $r_{3bs}$  and  $r_{3bg}$  being the radius of the beam stop and the radius of the image of the central beam projected on the beam-stop plane, respectively;  $r_{4\min} = r_{4bs} + r_{4bg}$ , where  $r_{4bs}$  and  $r_{4bg}$  are the radius of the beam stop projected on the detector plane and the radius of the image of the central beam projected on the detector plane, respectively. Under the ideal conditions when the beamstop radius is exactly the radius of the direct beam  $r_{3bs} = r_{3bg}$  and  $r_{4bs} = r_{4bg}$ ,

$$r_{3\min} = 2r_{3bs} = 2r_{3bg} = L_2(d_1 + d_2)/L_1 + d_2 \quad (3a)$$

$$r_{4\min} = 2r_{4bs} = 2r_{4bg} = (L_2 + L_3)(d_1 + d_2)/L_1 + d_2. \quad (3b)$$

The actual resolution achieved, determined by  $r_{4\min}$ , depends on the beam geometry, the parasitic scattering and in turn on the practical beam-stop size, as well as on the finite, asymmetric dimensions of the pixels. Thus, the parameter  $r_{4\min}$  can be expressed as the sum of the radius of the beam stop ( $r_{3bs}$ ) projected onto the detector plane  $r_{4bs} = (L_2 + L_3)r_{3bs}/L_2$ , the radius of the image of the direct beam projected onto the detector plane  $r_{4bg} = 0.5[(L_2 + L_3)(d_1 + d_2)/L_1 + d_2]$ , and the semi-diagonal length of a pixel  $0.5(p_x^2 + p_y^2)^{1/2}$ :

$$r_{4\min} = r_{4bs} + r_{4bg} + 0.5(p_x^2 + p_y^2)^{1/2} \quad (4)$$

where  $p_x$ ,  $p_y$  are the pixel dimensions in the  $x$  and  $y$  directions, respectively. When  $L_1 = 1.0$  m,  $L_2 + L_3 = 2.33$  m,  $d_1 = 0.6$  mm and  $d_2 = 1.2$  mm, the calculated apparent beam diameter when projected onto the detector plane is  $2r_{4bg} + (p_x^2 + p_y^2)^{1/2} = 7.3$  mm larger than the apparent beam diameter measured from Fig. 2. When a beam stop of a diameter of 6 mm is installed, the calculated  $r_{4\min}$  according to equation (4) is 6.8 mm corresponding to  $Q_{\min} = 0.012 \text{ \AA}^{-1}$ . In a real solution

SAXS experiment, an effective  $Q_{\min}$  of  $0.01 \text{ \AA}^{-1}$  can usually be achieved, better than the calculated value.

In order to increase the flux at the sample with a given required resolution, we have adopted an asymmetric geometric configuration, that is, the ratio of the diameters of the two circular apertures  $a = d_2/d_1$  and the ratio of the sample-to-beam-stop distance to the collimator length  $b = L_2/L_1$  are both larger than unity. From equations (1), (2) and (3a), the flux at the sample can be expressed in terms of resolution  $R$  as defined in equation (2), and the parameters  $a$  and  $b$ :

$$F = B[(\pi^2 d_1^2)/16](d_2^2/L_1) \\ = \text{const}(1/R^2)[1 + (1/a) + (1/b)]^{-2}. \quad (5)$$

The term  $[1 + (1/a) + (1/b)]^{-2}$  is the efficiency  $E$  of obtaining flux with a given resolution  $R$  in a real system. In an ideal system with infinite  $a$  and  $b$ ,  $E = 1$ . Equation (5) shows that the flux is fundamentally proportional to  $R^{-2}$  and that the larger  $a$  and  $b$ , the nearer the approach to the limit. In the implementation presented here,  $a = 2$  and  $b = 1.93$ . Enlarging  $a$  enlarges the required  $L_1$  and enlarging  $b$  increases  $L_2$ . In practice  $L_1 + L_2 + L_3$  is limited by the space available, and the benefit of increasing  $a$  and  $b$  diminishes when they are large compared to 1. When  $a$  and  $b$  are each 1 as recommended by some authors (Hendricks, 1978), the efficiency term  $E = [1 + (1/a) + (1/b)]^{-2} = 1/9$ . In our design  $a = b \approx 2$ ,  $E = 1/4$ . Doubling  $a$  and  $b$  again would yield  $E = 4/9$ . To aid in an intuitive understanding of the above statement, consider the 'cross fire' angle of the collimator  $\alpha$  between extreme crossing rays (see Fig. 1a)

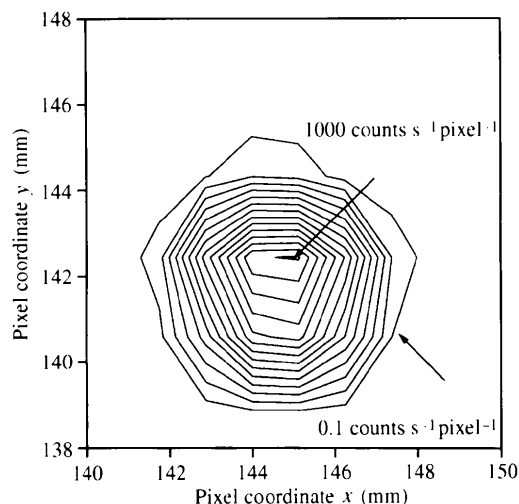


Fig. 2. The two-dimensional intensity profile of the attenuated direct beam using a linear contour spacing. The pixel coordinates are presented in mm. This circular-aperture-collimated beam is essentially symmetric and circular. The beam intensity was measured at  $L_1 = 1.0$  m,  $L_2 + L_3 = 2.33$  m,  $d_1 = 0.6$  mm,  $d_2 = 1.2$  mm. The X-ray generator was operated at 50 kV, 20 mA and the beam was attenuated by a total nickel foil thickness of 0.127 mm.

and the resolution-determining angle  $\beta = 2r_{3bg}/L_2$ . It is apparent that  $\alpha < \beta$ . As  $b \rightarrow \infty$ ,  $\beta \rightarrow \alpha$ . If the second aperture ( $d_2$ ) is moved outward along the cross-fire extreme rays,  $\alpha$  will remain constant and the flux will increase since  $d_2$  increases more rapidly than  $L_1$ . Conversely, shortening the collimator will reduce  $d_2$  more rapidly than  $L_1$  and the flux will be lost.

The brilliance  $B$  per source power and per entrance aperture area of the direct beam was determined by measuring the X-ray intensities passing through different numbers of layers of nickel foil and extrapolating the linear region of the semi-log plot to zero thickness (see Fig. 3). Principally, the intensity of the integrated direct beam does not depend on the sample-to-detector distance, but a 25 cm air gap as shown in Fig. 1(a) and 1(b) in the sample-to-detector path is responsible for some loss in the total flux (a 25 cm air gap reduces the total flux by about 23%). The detector efficiency has been estimated to be 50% (Hamlin, 1985). After correction for the detector efficiency and air absorption, the brilliance  $B$  per source power and per entrance aperture area was  $9.8 \times 10^{12}$  counts  $s^{-1}$   $mm^{-2}$   $kW^{-1}$ , which was slightly lower than the  $1.1 \times 10^{13}$  counts  $s^{-1}$   $mm^{-2}$   $kW^{-1}$  value of the SAXS system at ORNL (Wignall *et al.*, 1990).

The sample-scattered intensity may be maximized by an appropriate selection of the sample thickness  $t$ . In equation (1) the scattered intensity from the sample is proportional to  $t \exp(-\mu_s t)$ . This  $t \exp(-\mu_s t)$  term

reaches a maximum value at a sample thickness  $t_{max} = 1/\mu_s$  (see Fig. 4). For a protein buffered in an aqueous solution ( $\mu_s \approx 1.0$   $mm^{-1}$  for Cu  $K\alpha$ ),  $t_{max} = 1.0$  mm; when measuring the chemical denaturation of a protein in a 2 M guanidine hydrochloride solution ( $\mu_s \approx 1.7$   $mm^{-1}$  for Cu  $K\alpha$ ),  $t_{max}$  is about 0.6 mm.

The choice of the sample thickness  $t$  is also affected by considerations of the ratio of sample scattering to parasitic scattering and the counting statistics at a fixed data-collection time. According to equation (1), the parasitic scattering term is proportional to  $\exp(-\mu_s t)$  and the ratio of the sample scattering to the parasitic scattering is proportional to the sample cell thickness  $t$  provided that the solvent scattering is relatively small. A thicker sample size absorbs more of the parasitic scattering and increases the sample scattering to parasitic scattering ratio. However, if the sample cell is too thick,  $t \exp(-\mu_s t)$  may become very small and the data collection time becomes unacceptably long to achieve a desired counting error. Fig. 4 shows that in an aqueous buffer solution, the calculated  $t \exp(-\mu_s t)$  is reduced by about 27% from its maximum value when  $t$  is changed from 1 to 2 mm while the calculated parasitic scattering is decreased by about 65% and the ratio of sample scattering to parasitic scattering is increased twofold. Fig. 5(a) gives the actual scattering data  $I(Q)$  of a bovine serum albumin (BSA) protein solution in 1 and 2 mm thick cells. The scattering intensity was reduced by about 25–30% in the small-angle region when  $t = 2$  mm, but the effect on counting statistics was negligible when  $t = 2$  mm (see Fig. 5b).

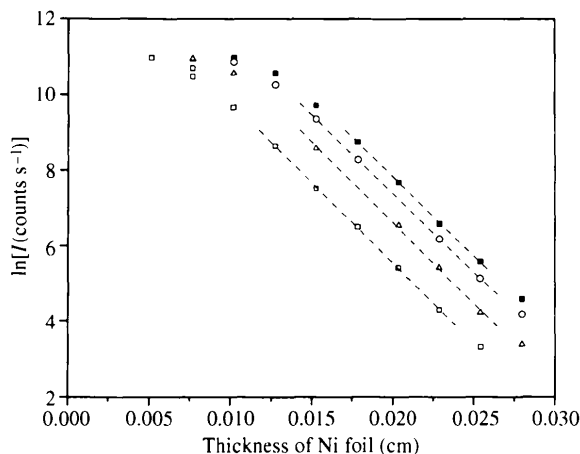


Fig. 3. The natural logarithmic intensity of the integrated direct beam as a function of nickel foil thickness at four source powers ( $\square$ : 50 kV, 20 mA;  $\triangle$ : 50 kV, 60 mA;  $\circ$ : 50 kV, 120 mA;  $\blacksquare$ : 50 kV, 180 mA). At the operating source power of 50 kV, 180 mA, the intensity of the integrated beam is  $1.1 \times 10^7$  counts  $s^{-1}$  obtained by extrapolating the linear region to zero nickel foil thickness. 15 pixels were used to determine the intensity of the direct beam at each foil thickness. These intensities were measured when  $d_1 = 0.6$  mm,  $d_2 = 1.2$  mm,  $L_1 = 1.0$  m,  $L_2 + L_3 = 2.33$  m. The rotating anode had not been polished for 2000 h when these intensity data were collected (a freshly polished anode will give increased intensity). The intensities are presented without correcting for detector efficiency.

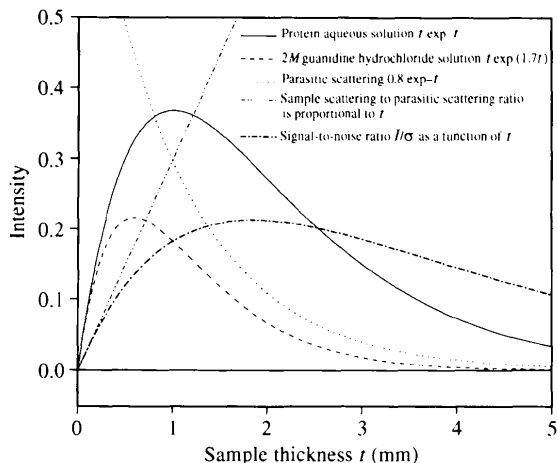


Fig. 4. The effect of sample thickness on the scattered intensity. In aqueous solution, the  $t \exp(-\mu t)$  term in equation (1) reaches a maximum at a sample thickness of  $t_{max} = 1.0$  mm. In a 2M guanidine hydrochloride solution,  $t_{max}$  is about 0.6 mm. Note the sample thickness is 2 mm, thicker than  $t_{max}$ , to reduce the parasitic scattering and to improve the sample scattering to parasitic scattering ratio twofold. The parasitic scattering curve is on an arbitrary scale. The actual instrumental background is usually larger than the net sample scattering.

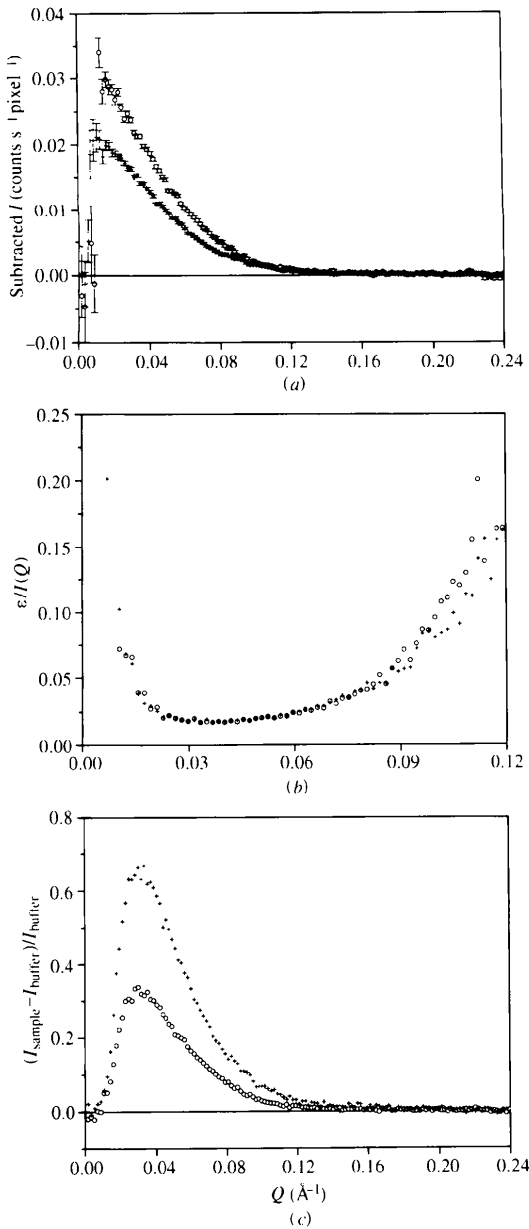


Fig. 5. (a) The subtracted scattering data  $I(Q)$  of  $5 \text{ mg ml}^{-1}$  BSA in  $150 \text{ mM NaCl}$ ,  $10 \text{ mM tricine}$  buffer solution in sample cells of thickness of (○) 1 and (+) 2 mm. The sample cells have parallel windows made of 0.1 mm polystyrene film. In both cases the data-collection times are 2 h for the protein solution and the buffer, respectively. The data are circularly averaged with the annulus of width 1 mm centered at the integral beam center. The first point shown here is at 1 mm radius. (b) The effect of changing sample thickness on counting errors of the scattering from the  $5 \text{ mg ml}^{-1}$  BSA solution. The counting errors are not affected significantly when the sample cell thickness is changed from (○) 1 and (+) 2 mm. The first point is at 5 mm radius since the  $\varepsilon/I$  ratio of those points below 5 mm radius is negative and meaningless. (c) The protein scattering to background scattering ratio presented as  $[I(Q)_{\text{sample}} - I(Q)_{\text{buffer}}]/I(Q)_{\text{buffer}}$  as a function of  $Q$  of the  $5 \text{ mg ml}^{-1}$  BSA solution in sample cells of thickness (○) 1 and (+) 2 mm. The first point shown here is at 1 mm radius.

When the buffer background scattering is high compared to the instrument parasitic scattering, the effect of increasing the sample thickness on improving the macromolecule scattering to the total background scattering ratio may be discounted. However, in the scattering results shown in Fig. 5 the buffer scattering contributed less than 10 and 20% of the total background scattering when  $t = 1$  and 2 mm, respectively. Fig. 5(c) shows that the actual protein scattering to total background scattering ratio is increased about twofold in the small-angle region when  $t$  is changed from 1 to 2 mm.

The signal-to-noise ratio  $I/\varepsilon$ , *i.e.* the subtracted scattering intensity to the counting statistics, can be calculated from equation (1) as

$$\begin{aligned} I/\varepsilon &= \frac{B_b G T_b t [\sigma_s(Q) - \sigma_b(Q)]}{2^{1/2} [B_b G T_b t \sigma_b(Q) + B_b T_b \Pi_b(Q)]^{1/2}} \\ &= \text{Const} \frac{t \exp(-\mu_b t/2) [\sigma_s(Q) - \sigma_b(Q)]}{[G t \sigma_b(Q) + \Pi_b(Q)]^{1/2}} \quad (6) \end{aligned}$$

where  $\varepsilon = (\varepsilon_b^2 + \varepsilon_s^2)^{1/2} \simeq (2\varepsilon_b)^{1/2} = \{2[B_b G T_b t \sigma_b(Q) + B_b T_b \Pi_b(Q)]\}^{1/2}$  [see equations (8) and (9) for buffer subtraction]. According to equation (6), the sample thickness  $t$  at which  $I/\varepsilon$  reaches a maximum depends on the relative magnitude of the parasitic scattering term to the net sample scattering term. Fig. 4 also shows that the calculated  $I/\varepsilon$  reaches a maximum value at  $t \simeq 1.9$  mm when the parasitic scattering term is assumed to be tenfold stronger than the net sample scattering term, which is usually the case for the SAXS system reported here. Thus, changing  $t$  from 1 to 2 mm reduces the parasitic scattering and improves the macromolecule scattering to background scattering ratio which in turn reduces any systematic error resulting from scaling errors during buffer subtraction. When measuring a protein dissolved in a routine buffer, *e.g.* a buffer of 0–250 mM NaCl, we recommend a 2 mm thick sample cell.

## 2.2. Reducing background scattering

A well collimated beam with minimum parasitic scattering will improve the resolution. At the edge of the beam stop, it is typically desirable to have non-sample scattering  $I_p$  less than  $10^{-6}$  times the central beam  $I_o$ . The foil used to form the beam-defining aperture should be thick enough to block the unwanted X-rays, but should not be too thick since a thicker aperture may cause more parasitic scattering by reflecting X-rays from the edge of the defining aperture (see Fig. 6). If the aperture is a perfect cylinder, the reflected X-rays would be blocked by the beam stop. When the aperture is not a perfect cylinder, the reflected X-rays may contribute to the parasitic scattering. The beam-defining aperture  $d_2$  with a thickness  $\tau$  will potentially reflect X-rays in the forward direction with a foreshortened reflective area of  $A_{\text{reflective}} = \pi d_2 \tau (d_2/2L_1)$ . The ratio of the intensity of the

total reflected X-rays to that of the direct beam exiting the collimator is  $I_{\text{reflective}}/I_o = \pi d_2 \tau (d_2/2L_1) / (\pi d_2^2/4) = (2\tau/L_1)$ , independent of the aperture diameter.

We have selected platinum foil to form the beam-defining aperture. Since platinum foil has a larger linear absorption coefficient of Cu  $K\alpha$  ( $\mu_{\text{Pt}} = 429 \text{ mm}^{-1}$ ) than lead foil ( $\mu_{\text{Pb}} = 263 \text{ mm}^{-1}$ ), a thinner platinum foil is sufficient to block the unwanted X-rays relative to the lead foil. Platinum foil of  $50 \mu\text{m}$  thickness used in our SAXS station attenuates the direct beam  $4.8 \times 10^{-10}$  fold. The  $I_{\text{reflective}}$  to  $I_o$  ratio of any diameter aperture made of such platinum foil is  $10^{-4}$  in a 1 m collimator. Fig. 7 shows the measured background scattering intensity in counts  $\text{s}^{-1} \text{ pixel}^{-1}$  in the  $0 \leq Q \leq 0.1 \text{ \AA}^{-1}$  region. The ratio of the background scattering intensity in counts  $\text{s}^{-1} \text{ pixel}^{-1}$  to the intensity of the integrated directed beam in the  $0 \leq Q \leq 0.1 \text{ \AA}^{-1}$  region was less than  $1.2 \times 10^{-6}$ .

The scattering of X-rays by air has two effects. Air scattering and absorption reduce X-ray intensity by about 1% per centimeter. Also, air scattering between the sample and the beam stop would dominate the background noise. We have selected to flush the entire monochromator housing, the collimator and the sample-to-beam-stop paths with helium to reduce air scattering and absorption. The 40 cm gap between the beam stop and the detector markedly reduces the background scattering from helium in the sample-to-beam-stop path reaching the detector compared to placing the detector immediately following the beam stop. This is because each element of helium contributes to the background scattering proportionally to the inverse square of the distance to the detector. The integral background scattering from the whole path up to the beam stop is approximately proportional to the inverse of the beam-stop-to-detector distance  $1/L_3$ . This design feature is not new (see, for example, Guinier & Fournet, 1955, pp. 124–125; Kratky *et al.*, 1951).

### 2.3. Beam monitor

The Bragg reflection peaks of a polycrystalline ammonium sulfate pellet are used to monitor the beam intensity and sample absorption in our SAXS station. Crystalline ammonium sulfate has orthorhombic cell dimensions of  $a \times b \times c = 5.98 \times 10.62 \times 7.78 \text{ \AA}$ . When co-precipitated with corn starch by adding an aqueous

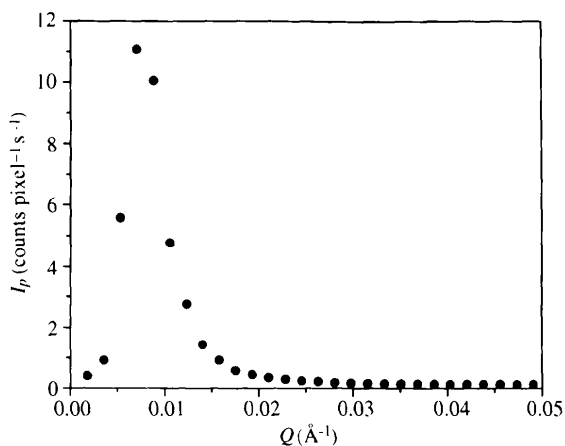


Fig. 7. The intensity of background scattering in counts  $\text{s}^{-1} \text{ pixel}^{-1}$  as a function of  $Q$ . The intensity of the integrated direct beam is  $I_o = 1.1 \times 10^7$  counts  $\text{s}^{-1}$ . The solid angle of a pixel as seen from the sample is  $4.1 \times 10^{-7}$  steradians. The first point shown is at 1 mm radius.

solution to ethanol, a fine crystalline powder of ammonium sulfate is obtained, which can be compressed into a circular pellet. The diameter of the pellet is a little smaller than that of the beam stop. This pellet diffracts three powder rings on the area detector when placed 2.5 cm in front of the beam and 42.5 cm in front of the detector (see Fig. 8).

## 3. Description of the apparatus

### 3.1. The SAXS station

The X-ray source is a Rigaku-RU 300 rotating-anode generator with a copper target producing  $1.54 \text{ \AA}$  characteristic X-rays. The dimensions of the electron beam at the target are  $10 \times 0.5 \text{ mm}$  and the take-off angle  $\gamma$  is  $12^\circ$ . When the generator operates at 9 kW ( $50 \text{ V} \times 180 \text{ mA}$ ), the average lifetime of the filament is about 2000 h. The generator could be run at 12 kW with reasonable performance but we have conservatively stopped at 9 kW.

The total length of the SAXS station is 3.33 m. The graphite monochromator can be rotated around a vertical axis to obtain Bragg reflection, tilted to adjust for the source elevation and translated to adjust for the horizontal displacement. The monochromator is enclosed in a helium-flushed housing. The output port of

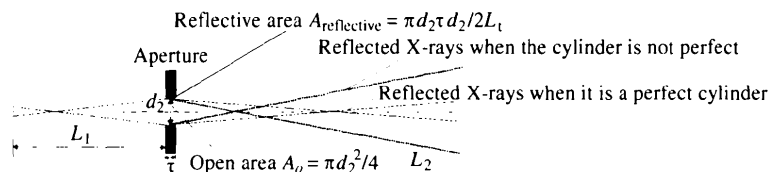


Fig. 6. The thickness of the aperture affects the amount of the reflected X-rays. A defining aperture  $d_2$  with a thickness  $\tau$  reflects X-rays in the forward direction from the surface edge of the aperture. The reflected X-rays from an imperfect cylinder contribute to the parasitic scattering. The ratio of the scattered X-rays to the direct beam is equal to the ratio of the foreshortened reflecting area to the area of the open aperture.

the monochromator is the input aperture of the collimator  $d_1$ , producing a partially pre-collimated beam. When the filament is replaced, the source displacement is small enough so that the beam intensity is reduced by 10–30% but not lost. Adjustments of the monochromator suffice to restore quickly maximum flux and adjustment can be completed in a few minutes.

The detector is a two-dimensional San Diego Multi-wire Systems (SDMS) detector (Hamlin, 1985) with  $256 \times 144$  pixels and a sensitive area of  $290 \times 288$  mm. Each impinging X-ray photon is assigned to a single pixel of dimensions  $\Delta y \times \Delta z = 1.125 \times 2$  mm. Important characteristics of the SDMS detector are its stability, uniformity and high quantum yield. The total dark count is about 60 counts  $s^{-1}$  or less. On our SAXS station the photon-counting rate is usually between 1000 and 3000 counts  $s^{-1}$ , much lower than the maximum counting rate of the detector. The detector can be translated in the  $xy$  plane as shown in Fig. 1(b).

The collimator is a helium-flushed brass tube. Its design is shown in Fig. 9. The diameter of the first

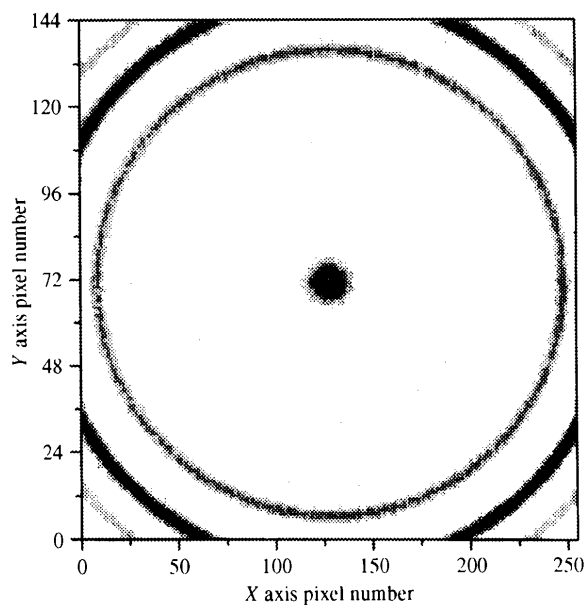


Fig. 8. The two-dimensional diffraction pattern of the polycrystalline ammonium sulfate pellet used as an online beam monitor. The sample is a 150 mM NaCl, 10 mM tricine, pH 7.9 buffer in a 2 mm thick cell with parallel polystyrene film windows. The two weak rings at intermediate angles are diffraction by the beam monitor of  $\lambda/2$  contamination of the main beam originating in the white radiation from the source. Wavelengths of  $\lambda/2$ ,  $\lambda/3$ , etc. are diffracted by the monochromator at the same angle as  $\lambda$  in the second and third order, etc. These radiations are inherently weak but are enhanced relative to  $Cu K\alpha$  by differential transmission through the beam-monitor pellet. Their intensity in the sample scattering is negligible and their presence in the beam-monitor diffraction pattern is of no serious consequence since they are properly subtracted out along with the  $Cu K\alpha$  peaks.

aperture is  $d_1 = 0.6$  mm. Because all the collimator parts are fastened together by 'O' rings, depending on the requirement of an experiment, the collimator can be readily assembled and disassembled to change the length of the collimator  $L_1$  and the aperture sizes  $d_1$  and  $d_2$ . The size of the second aperture  $d_2$  can be varied by exchanging a pre-machined aperture glued on an exchangeable button as shown in Fig. 9. The collimator is supported near the sample holder by two  $xy$  plane-positioning micrometers facilitating precise adjustment.

The diameter of the collimator tube is chosen to be 32 mm in this case so that the pre-collimated beam from the monochromator does not strike the wall of the tube; if marginal X-rays do strike the wall, the angle of incidence will be many times the critical angle for total reflection. This effectively reduces parasitic scattering. Possible fluorescence is additionally reduced by selecting a brass tube since  $Cu K\alpha$  does not excite Cu.

The aperture  $d_2$  is formed by clamping a piece of 50  $\mu m$  thick platinum foil (purchased from Aldrich, cat. No. 34, 935-6) between two brass plates and then drilling through with a sharp drill. This produces a clean hole with low parasitic scattering. Platinum was chosen because the high density and high absorption coefficient for  $Cu K\alpha$  allow the use of a thin foil. The scattering from the entrance aperture is not critical, so a hole drilled in a simple, thick brass button is adequate. Fluorescence from the brass is of no concern.

A cone of rectangular cross section made with 5 mm thick polyvinyl chloride sheet (to absorb stray X-rays) and having a 0.1 mm thick polystyrene film entrance window and a mylar film exit window provides a helium path between the sample and the beam stop. The cone is mounted on a  $z$  translator which also carries an  $xy$  translator for the beam stop and beam monitor assembly. The cone is skewed so that the detector can be centered on the beam or translated to the wider side to collect a larger angular range of the scattered intensity without changing the apparatus configuration. The sample-to-detector distance can be varied from 0.5 to 2.3 m by changing the helium cone to one with a different length. The total reconfiguration time is about 30 min by one experienced operator when the optical configuration is changed completely.

The sample holder is mounted on an  $xy$  two-dimensional translator. A 2.0 mm quartz capillary tube is

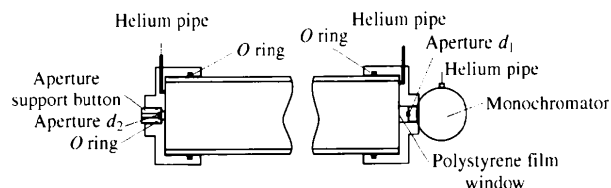


Fig. 9. Diagram of the collimator design.

inserted and glued in the sample holder. A glass capillary tube may scatter X-rays less than a quartz capillary but is much more fragile. The observed scattering from either the quartz or the glass capillary tube is much smaller than our total instrument background. The temperature of the sample holder is controlled with a circulating water bath. This sample holder requires about 10–50  $\mu\text{l}$  sample solutions. When a measurement is finished, the sample solution can be pipetted out and the same quartz capillary tube reused without changing its position. All the sample solutions and the solvents in a series of samples are measurable without changing such instrument factors as the position and the path length of the sample. Keeping these instrument factors unchanged throughout the series is important with respect to ensuring a correct background subtraction and correct interpretation of the scattering data. Cells of path lengths 2, 1.5 and 1 mm with parallel windows made of 0.1 mm polystyrene film are useful for samples of increasing absorbency.

The direct beam is blocked by a brass beam stop, 6 mm in diameter. The beam monitor was made as follows. A 50 ml 28.8% (*w/v*) aqueous solution of ammonium sulfate and 0.02% corn starch was boiled and diluted with water to 75 ml. A 25 ml aliquot of that solution was added to 200 ml of 100% ethanol to coprecipitate the ammonium sulfate and the corn starch. The white precipitate was collected *via* vacuum filtration and allowed to dry in air. The ammonium-sulfate–corn-starch coprecipitate was added to a 5 mm diameter brass mold and hand pressed with a small arbor press into a polycrystalline pellet. The thickness of the pellet was 1 mm and the density of the beam-monitor pellet was  $1.6 \text{ g cm}^{-3}$ . Since the beam monitor was calculated to attenuate the central beam 104-fold, the scattering from air between the monitor and the beam stop is insignificant and this beam-monitor/beam-stop assembly does not need to be in the helium chamber.

The polycrystalline ammonium sulfate pellet is installed about 2.5 cm in front of the beam stop to intercept the X-ray beam and diffract three rings on the area detector. The detector is placed about 40 cm beyond the beam stop so that the (110) reflection from the polycrystalline pellet falls near the edges of the area detector, and the (111) and (002) reflections fall in the corners. The intensity of the powder diffraction pattern from this pellet is used as an internal monitor of the changes in beam intensity and absorption/transmission in X-rays by the sample. The location of the beam-monitor-diffracted peaks is  $0.21 < Q < 0.32 \text{ \AA}$ , which does not interfere with the  $Q$  range of interest. Both the beam stop and the beam monitor are mounted on polystyrene films glued to a frame. The frame can be translated in the *xy* plane to adjust the position of the beam stop and the beam monitor when aligning the instrument.

### 3.2. Detector–computer interface, data acquisition

The SDMS detector electronics produce a 16 bit data output (8 bits each for *y* and *z* coordinate), along with handshaking control signals. The detector electronics can be interfaced to a Digital Equipment Corporation VAXstation 3200 computer with a DRQ3B parallel DMA (direct memory access) I/O module (Digital Equipment Corporation, 1989). The DRQ3B accepts the TTL (transistor–transistor logic) data and controls signals from the Area-Detector System Corporation (ADSC) electronics, buffers the data internally, and transfers full buffers to the computer using DMA.

A program running on the VAXstation plots the data as a histogram in the computer memory, *i.e.* a counter is maintained for each of the  $144 \times 256$  pixels in the detector, and is incremented each time a photon is reported at that pixel coordinate. The program saves the plotted data to a disk file at regular intervals. Other programs start and stop data collection, display data (locally or on a remote X-Windows server), control the X-ray shutter and the constant-temperature bath. Data can then be processed locally, or transferred to another computer for further processing.

Some data are lost if two photons impinge anywhere on the detector with insufficient delay. Hamlin (1985) gives the fraction  $f(r)$  lost in this manner as

$$f(r) = 1 - \exp[-R(2T_1 + T_2)] \quad (7)$$

where  $R$  is the raw photon detection rate,  $T_1$  is the maximum detector delay line time, and  $T_2$  is the time required to transfer a coordinate pair to the DRQ3B module.  $T_1$  is given by Hamlin as  $2 \mu\text{s}$ ,  $T_2$  is less than  $0.5 \mu\text{s}$  (Digital Equipment Corporation, 1989); at typical data rates of  $2000 \text{ counts s}^{-1}$ , the loss is less than 1%. System diagnostic tools running on the VAXstation indicate that the computer's processing capacity is used at a rate of less than 10% at  $2000 \text{ counts s}^{-1}$ . Although it is obsolete by today's standards, the VAXstation has proved a stable platform for this application. By using it to histogram the data, we avoid the expense and relative complexity of CAMAC (computer automated measurement and control) electronics, which are usually used to histogram and control the SDMS detector.

### 3.3. Data reduction and analysis

No correction for detector nonuniformity has been found necessary on the SDMS detector as judged from the scattering image and the quality of the reduced data. Since the beam is pinhole collimated, it can be treated as point-like, and no desmearing of the scattering data is therefore necessary on this SAXS apparatus. To prove this point, a frame of the attenuated direct beam was collected and fed into the *GNOM* program (Semenyuk & Svergun, 1991) to calculate the length distribution function  $P(r)$  of  $5 \text{ mg ml}^{-1}$  BSA in  $150 \text{ mM NaCl}$ ,  $10 \text{ mM}$  tricine buffer. The *GNOM* software has the

options of calculating the  $P(r)$  function and the radius of gyration assuming the experiment condition has no smearing, or desmearing with a given direct-beam intensity profile measured without the beam stop and the sample. The  $P(r)$  functions and the radii of gyration of the measured BSA with and without desmearing of the intensity profile were essentially the same.

A program package, *ANSAXS*, has been developed to reduce the scattering data. The two-dimensional 16 bit data are circularly and time averaged and reduced to  $I(Q)$  in counts pixel<sup>-1</sup> s<sup>-1</sup> versus  $Q$  plots. Multiple scans on the sample or the blank can also be summed and averaged at the same time. For oriented, anisotropic samples, the program has the option of performing averaging within a specified angular range about the origin in the detector plane. With the aid of the peak intensity diffracted from the beam monitor, the linear scattering data can be normalized to correct for the beam-intensity changes and absorption/transmission differences and subtracted to obtain the net corrected scattering data  $I(Q)$ . A program for extrapolating finite-concentration scattering data to infinite dilution has also been developed. The principles of eliminating concentration effects are described by Tanford (1961) and Glatter & Kratky (1982). The scattering data are then further reduced to a  $\ln I(Q)$  versus  $Q^2$  plot (Guinier plot) and a  $1/I$  versus  $Q^2$  plot (Zimm plot) for small-angle analysis and the Kratky  $I(Q) \cdot Q^2$  versus  $Q$  plot for larger-angle analysis.

The principles of normalization and subtraction of the scattering data are as follows. The measured intensity  $I(Q)$  is a sum of the scattering from the sample  $B_s G T_s \sigma(Q)$ , the parasitic scattering  $\Pi(Q)$  and the dark count Dark as described in equation (1) (subscript  $s$  stands for the sample solution, and  $b$  for the solvent alone). The dark count is generally low on the SDMS area detector used here and can be assumed to be time independent so that  $D_s = D_b$ . The parasitic scattering term  $\Pi(Q)$  can also be assumed to be the same for the sample and the solvent because no instrument factors were changed during the measurements. The peak areas, above a baseline level, of all three rings diffracted by the beam monitor are

$$\begin{aligned} A_s &\propto I_s(0) = B_s G T_s \\ A_b &\propto I_b(0) = B_b G T_b \end{aligned} \quad (8)$$

for the sample solution and the solvent, respectively. After  $I_s(Q)$  is scaled with a factor  $(A_b/A_s) = [(B_b T_b)/(B_s T_s)]$  to correct for the beam intensity and the transmission difference, the subtracted intensity  $I(Q)$  is

$$I(Q) = B_b G T_b t[\sigma_s(Q) - \sigma_b(Q)] = B_b G T_b t \sigma(Q) \quad (9)$$

where  $\sigma(Q)$  is the scattering cross section of the macromolecules. Since the scale factor is near unity when measuring a dilute protein buffer, both the parasitic and the dark-current terms cancel. In the absence of

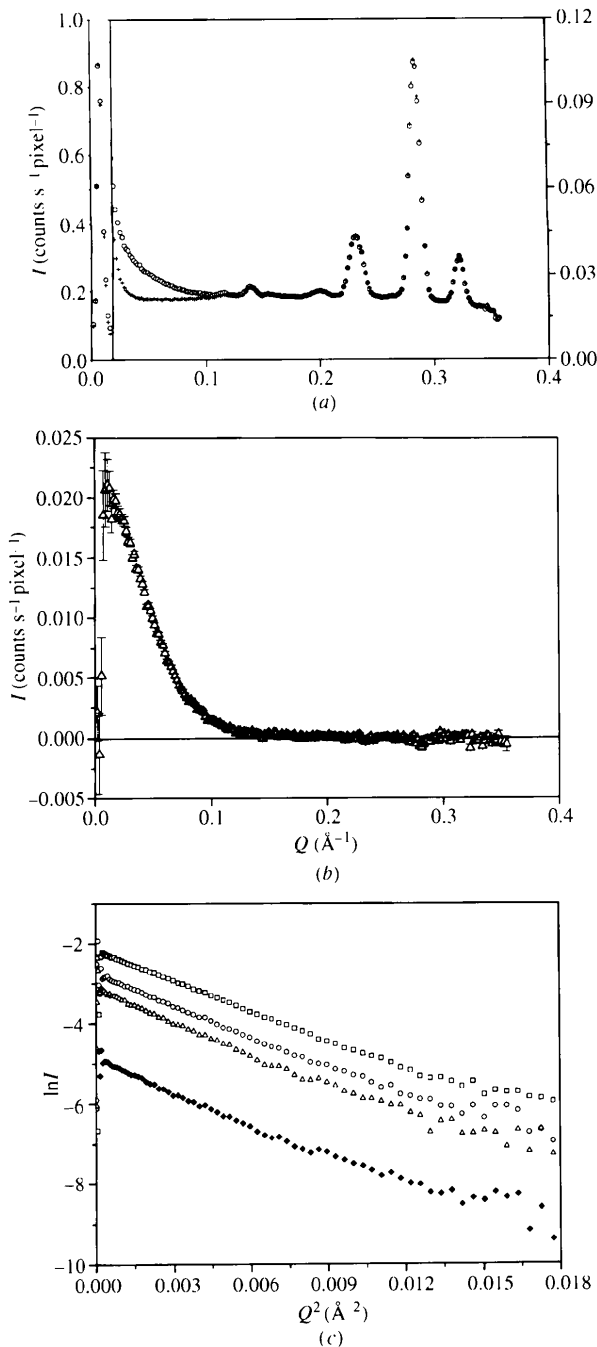


Fig. 10. (a) The linear scattering profile from a 5 mg ml<sup>-1</sup> BSA in 150 mM NaCl, 10 mM tricine, pH 7.9 solution (○, solution; +, buffer). Shells arc at 1 mm intervals on the detector. The first point is at 0.1 mm radius from the center of the direct beam. The small shoulders at around  $Q = 0.12, 0.14$  and  $0.2$  Å<sup>-1</sup> are explained in the legend of Fig. 8. Their effect on the net scattering data is negligible after buffer subtraction. (b) The subtracted scattering data  $I(Q)$  versus  $Q$  of the sample shown in Fig. 10(a) (△, 5 mg ml<sup>-1</sup> BSA). (c) Guinier plots of BSA, in 150 mM NaCl, 50 mM NaH<sub>2</sub>PO<sub>4</sub> solution at (○) 18.24 mg ml<sup>-1</sup>,  $R_g = 27.3$  (2) Å; (□) 9.12 mg ml<sup>-1</sup>,  $R_g = 28.8$  (3) Å; (△) 6.08 mg ml<sup>-1</sup>,  $R_g = 29.7$  (4) Å; and (●)  $\ln[I(Q)/c]$  at  $c \rightarrow 0$ ,  $R_g = 29.6$  (5) Å.

intermolecular interaction effects,  $\sigma(Q)$  can be expressed as (Pessen *et al.*, 1973; Glatter & Kratky, 1982; Moore, 1982)

$$\sigma(Q) = Ec(\rho_2 - \rho_1)^2 \bar{v}_2^2 M_w / N_a P(Q) \quad (10)$$

where the constant  $E$  is related to the scattering of a single electron;  $c$ ,  $\bar{v}_2$ ,  $M_w$ ,  $\rho_2$  and  $P(Q)$  are the concentration, the partial specific volume, the molecular weight, the electron density and the form factor of the measured macromolecules, respectively; and  $\rho_1$  is the electron density of the solvent. The form factor  $P(Q)$  can be approximated as (Guinier & Fournet, 1955)

$$P(Q) = \exp(-R_g^2 Q^2 / 3) \quad (11)$$

in the small-angle region and  $P(Q)$  is unity at  $Q = 0$ . The radius of gyration and the molecular weight can be obtained from the slope and the intercept of an  $\ln I(Q)$  versus  $Q^2$  plot (the Guinier plot), respectively. Since it is easy to obtain a monodisperse protein molecular-weight standard, such a standard can be used to calibrate the geometric factor and the intensity of the X-ray beam in equation (9) to measure a protein of unknown molecular weight.

#### 4. Application examples

Fig. 10(a) gives the circularly averaged raw scattering data of a 5 mg ml<sup>-1</sup>, 67 kDa BSA solution and its buffer. The sample cell is 2 mm thick with parallel polystyrene film windows. Data collection times were 2 h for both the sample solution and the buffer. The three large peaks from  $Q = 0.229$  to  $0.322 \text{ \AA}^{-1}$  are the diffraction

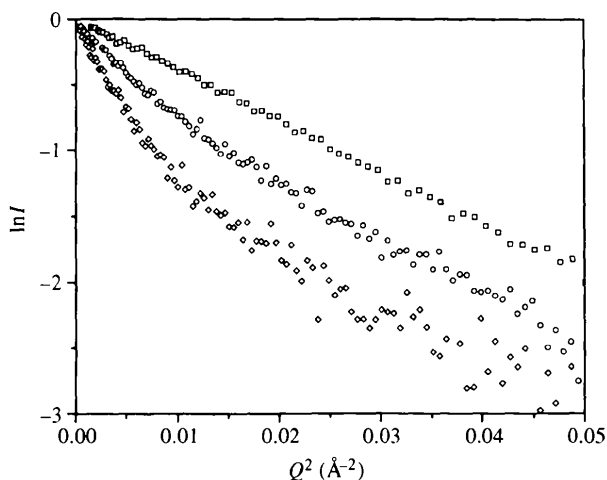


Fig. 11. Normalized Guinier plots of the 5 kDa B1 domain of streptococcal protein *G* at different GuHCl concentrations buffered in 50 mM sodium acetate, pH 5.2. (□) 10 mg ml<sup>-1</sup> protein at 0 M GuHCl, (○) 5.7 mg ml<sup>-1</sup> at 0.7 M GuHCl and (◇) 12.7 mg ml<sup>-1</sup> protein at 1.9 M GuHCl. The Guinier plots show this protein is progressively denatured as the GuHCl concentration is increased (Smith *et al.*, 1996).

pattern of the direct beam by the beam monitor. The total peak area of the three peaks was used to determine the scaling factor used in equations (8) and (9) for buffer subtraction. Fig. 10(b) shows the linear scattering data of the 5 mg ml<sup>-1</sup> BSA solution after buffer subtraction. The effective  $Q$  range is from 0.01 to  $0.3 \text{ \AA}^{-1}$ . The counting error of the subtracted scattering data in the small-angle region is shown in Fig. 5(b).

Fig. 10(c) shows the Guinier plots of scattering from BSA in 150 mM NaCl, 50 mM NaH<sub>2</sub>PO<sub>4</sub> solutions at different concentrations. These data were collected in a cylindrical 2 mm thick quartz capillary cell. The linearity of the Guinier plots suggests that the protein is monodisperse and globular. The radius of gyration of BSA from the scattering data extrapolated to  $c = 0$  from  $c = 18.24$ , 9.12 and 6.08 mg ml<sup>-1</sup> was 29.6 (5) Å, which is in good agreement with the literature value of 29.8 Å (Tanford, 1961). Since the partial specific volume of BSA is known, this protein is used as one of our molecular-weight standards to calibrate the X-ray beam when it is necessary to measure the absolute molecular weight of a protein or a protein complex.

Fig. 11 shows the Guinier plots of the denaturation of a small protein, the 5 kDa B1 domain of streptococcal protein *G*, as a function of guanidine hydrochloride (GuHCl) concentrations. This is a challenging measurement, both because the protein is small and because the electron-density contrast is low between the protein and the denaturant solutions. Solutions containing different denaturant concentrations were measured at a protein concentration of about 10 mg ml<sup>-1</sup>. Data collection times were 5 h for the folded protein and 24 h for the denatured proteins. The measured  $Q$  ranged from 0.013 to  $0.36 \text{ \AA}^{-1}$ . Guinier plots were fitted in the  $QR_g \leq 1$  region with a least-squares linear fitting routine. The radius of gyration changed from 10.8 (2) Å in the fully folded state to 23 (1) Å in the fully denatured state. The instrument proved stable, giving repeatable measurements in this difficult case.

We thank Dr D. I. Svergun for providing us with the *GNOM* program package for generating the  $P(r)$  functions, and Dr John Barnes of NIST for communications. This work was supported by an NIH grant to DME and HWW (GM22778). ZB is the recipient of an NIH NRSA postdoctoral fellowship (GM17364).

#### References

- Batenburg, A. M., van Esch, J. H. & de Kruijff, B. (1988). *Biochemistry*, **27**, 2324–2331.
- Digital Equipment Corporation (1989). *DRQ3B Parallel DMA I/O Module User's Guide*. Digital Equipment Corporation, Maynard, Mass., USA.
- Flanagan, J. M., Kataoka, M., Fujisawa, T. & Engelman, D. M. (1993). *Biochemistry*, **32**, 10359–10370.

- Glatter, O. & Kratky, O. (1982). *Small Angle X-ray Scattering*. London: Academic Press.
- Guinier, A. & Fournet, G. (1955). Editors. *Small-Angle Scattering of X-rays*. New York: John Wiley.
- Hamlin, R. (1985). *Methods in Enzymology*, Vol. 114, edited by H. W. Wyckoff, C. H. W. Hirs & S. N. Timasheff, pp. 416–452. Orlando, Florida: Academic Press.
- Hare, B. J., Prestigard, J. H. & Engelman, D. M. (1995). *Biophys. J.* **69**, 1891–1896.
- Hayashi, H., Hamada, F. & Suehiro, S. (1988). *J. Appl. Cryst.* **21**, 330–339.
- Hendricks, R. W. (1978). *J. Appl. Cryst.*, **11**, 15–30.
- Kataoka, M., Hagihara, Y., Mihara, K. & Goto, Y. (1993). *J. Mol. Biol.* **229**, 591–596.
- Kratky, O., Porod, G. & Kahovek, L. (1951). *Z. Elektrochem.* **55**, 53–59.
- Lattman, E. E. (1994). *Curr. Opin. Struct. Biol.* **4**, 87–92.
- Lemmon, M. A., Bu, Z., Ladbury, J. E., Zhou, M., Pinchasi, D., Lax, I., Engelman, D. M. & Schlessinger, J. (1997). *EMBO J.* **16**, 281–294.
- Lewis, B. A. & Engelman, D. M. (1983). *J. Mol. Biol.* **166**, 211–217.
- Moore, P. B. (1980). *J. Appl. Cryst.* **13**, 168–175.
- Moore, P. B. (1982). *Methods Exp. Phys.* **20**, 337–389.
- Pessen, H., Kumonsinski, T. F. & Timasheff, S. N. (1973). *Methods in Enzymology*, Vol. 27, edited by C. H. W. Hirs & S. N. Timasheff, pp. 151–209. New York: Academic Press.
- Rodgers, K. K., Bu, Z., Fleming, K. G., Schatz, D. G., Engelman, D. M. & Coleman, J. E. (1996). *J. Mol. Biol.* **260**, 70–84.
- Semenyuk, A. V. & Svergun, D. I. (1991). *J. Appl. Cryst.* **24**, 537–540.
- Smith, C. K., Bu, Z., Anderson, K., Sturtevant, J. M., Engelman, D. M. & Regan, L. (1996). *Protein Sci.* pp. 2009–2019.
- Tanford, C. (1961). *Physical Chemistry of Macromolecules*. New York: John Wiley.
- Tournois, H., Leunissen-Bijvelt, J., Haest, C. W., de Gier, J. & de Kruijff, B. (1987). *Biochemistry*, **26**, 6613–6621.
- Tuzikov, F. V., Zinoviev, V. V., Vavilin, V. I. & Malygin, E. G. (1996). *Biopolymers*, **38**, 131–139.
- Wignall, G. D., Lin, J. S. & Spooner, S. (1990). *J. Appl. Cryst.* **23**, 241–245.
- Yoda, O. (1984). *J. Appl. Cryst.* **17**, 337–343.